Scientific Research Publishing

Open Journal of Geology, 2024, 14, 81-100
https://www.scirp.org/journal/ojg
ISSN Online: 2161-7589
ISSN Print: 2161-7570

Mobility of Major and Trace Elements during the Bauxitization Processes in Ngaoundal Area (Adamawa Cameroon): Implication on Mining Perspectives

André Sini[1], Harouna Boukari[2], Ondoa Augustin Désiré Balla[3], Djetenbe Beral[3], Salomon Wangmené Awé[4], Simon Djakba Basga[5], Jean Pierre Nguetnkam[3]

[1]Department of Mining Engineering, School of Geology and Mining Engineering, University of Ngaoundere, Ngaoundere, Cameroon
[2]Department of Mining Engineering and Environment, School of Mining, Industry and Geology, University of Abdou-Moumouni, Niamey, Niger
[3]Department of Earth Sciences, Faculty of Science, University of Ngaoundere, Ngaoundere, Cameroon
[4]Department of Mining Engineering, Saint Jerome Polytechnic, Saint Jerome Catholic University Institute of Douala, Douala, Cameroon
[5]Institute of Agricultural Research for Development (IRAD), Garoua, Cameroon
Email: andrsini@yahoo.com

How to cite this paper: Sini, A., Boukari, H., Balla, O.A.D., Beral, D., Awé, S.W., Basga, S.D. and Nguetnkam, J.P. (2024) Mobility of Major and Trace Elements during the Bauxitization Processes in Ngaoundal Area (Adamawa Cameroon): Implication on Mining Perspectives. *Open Journal of Geology*, **14**, 81-100.
https://doi.org/10.4236/ojg.2024.141005

Received: October 28, 2023
Accepted: January 21, 2024
Published: January 24, 2024

Abstract

This study was focused to assess major and trace elements in bauxitic duricrusts from Ngaoundal and its surroundings in order to establish their mining interest. To this end, fieldworks, mineralogical and geochemical analyses were carried out. Four facies of duricrust were identified and characterized from the summit to the top of the slope of the Ngaoundal mountain: scoriaceous, pisolitic, nodular and massive. Mineralogical and geochemical analyses performed on 16 samples, revealed a significant concentration of Al_2O_3 mainly in the scoriaceous facies (over 45% in grade), moderate in Fe_2O_3 (averaging 23.69%) and SiO_2 (averaging 21.7%). Trace elements were generally low, excluding Cr (421 ppm on average), Zr (327 ppm on average and V (213 ppm on average). In addition, the limited quantities of alkalis (Na_2O, K_2O) and alkaline earths metals (MgO, CaO) coupled with the very high values of Chemical Index of Alteration (CIA) and Mineralogical Index of Alteration (MIA), (more than 99%) attest to the intense weathering of the studied materials. Allitization and monosiallitization constituted the crystallochemical phenomena that have led to the development of bauxitic minerals. More than 90% of gibbsite in scoriaceous facies, 52.21% - 76.01% of kaolinite in pisolitic facies and more than 40% of hematite in nodular facies were quantified. The rela-

tionships between the constitutive components indicated their interdependency during the bauxitization phenomenon. The mineralogical and geochemical properties highlighted the mining interest of the studied duricrusts to be valorized.

Keywords

Duricrust, Bauxitization Phenomenon, Mineralogical and Geochemical Characterization, Major and Trace Elements, Mining Potential

1. Introduction

Bauxites are residual or sedimentary rocks most often white, red or gray in color, with more than 40% of Al_2O_3, less than 10% SiO_2 and 20% Fe_2O_3 [1]. They are recognized as the main provider of aluminum. They are mainly formed under humid tropical to sub-tropical climates, with rainfalls in excess of 1200 mm and annual mean temperatures higher than 22˚C [2]. These materials play an important role in the economy of countries because they are the main resources of aluminum, and they may contain several critical elements, including rare earth elements [3]. Deposits are generally characterized into 3 major groups: lateritic bauxite deposits, karst bauxite deposits, and Tikhvin-type bauxite deposits [3]. The first group is the product of *in situ* and direct chemical weathering of alumino-silicate rocks lying beneath the surface. The second group is developed on the surface of more or less karstified carbonates (limestone and dolomite) and scarce marls. The third group is formed on the surface of eroded alumino-silicate rocks and is the erosional product of lateritic bauxite deposits. In Cameroon, several works on laterites in general, and lateritic bauxites in particular, were conducted [4] [5] [6] [7]. Some of these studies were focused on the characterization and evaluation of the well-known bauxites ores deposits in Minim Martap and Ngaoundal-Ngaoundouro in the Adamawa region [7] [8] [9], as well as in Fongo-Tongo and Bangam in the West region [6]. To ensure its emergence by 2035, it is essential for Cameroon to develop and appropriate geological knowledge of its subsurface. All this work contributed to a greater understanding of duricrust formations, but the available data are not sufficient to justify their entire mining potential. Furthermore, mineralogical and geochemical characteristics of the studied formations represent an important factor to control their mining properties. This study therefore focused on the behavior and the distribution of major and trace elements within duricrust formations from Ngaoundal and its surroundings, in order to assess their mining potential.

2. Materials and Methods

2.1. Study Area and Geological Settings

The studied area is located in zone 6˚22 and 6˚30 North Latitude and 13˚11 and 13˚18 East Longitude (**Figure 1**).

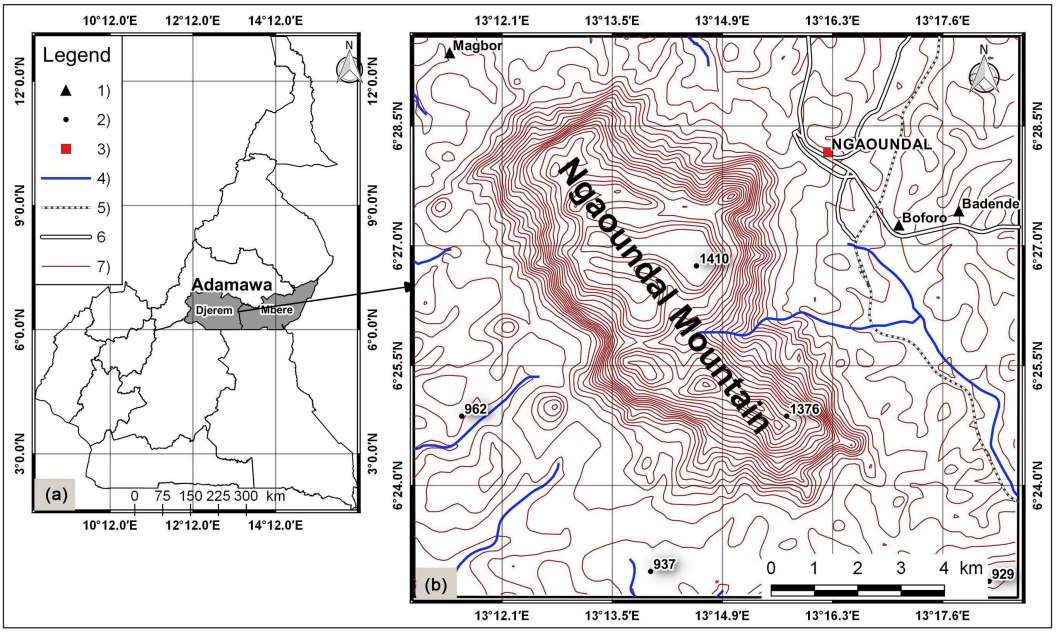

Figure 1. Location of study area. (a) Administrative map of Cameroon indicating the study area in Adamawa region. (b) Map of the study area obtained from 765 band of Landsat 8. 1) locality, 2) rated point, 3) Ngaoundal Town, 4) stream, 5) road, 6) railway, 7) level curve.

It is subjected to tropical Sudanese humid climate characterized by a long rainy season from March to October and short dry season from November to February [10]. The average annual rainfall is between 1500 and 1700 mm. The Sudano-Guinean anthropized savannah is the type of vegetation encountered in Ngaoundal [11]. The geomorphological features of the studied area are composed mainly of hills, with the Ngaoundal mountain which reaches an altitude of 1400 m. There are also some intermediate landforms made up of rolling land with some residual rises and plateaus that rarely exceed an altitude of 1100 m [12]. The slopes are steep and slightly inclined, separated by convexo concave interfluves coated by bauxitic duricrust formations, outcropping from the tops to the bottom of the hill.

From the geological point of view (**Figure 2**), the Ngaoundal sector belongs to the Central Cameroonian domain, also called the Adamawa-Yade domain of the Pan-African Chain of Central Africa [13] [14]. It includes Syn to late-tectonic granitoïds [15], partially overlain by basaltic, trachytic and phonolitic flows [16]. In this region, the bauxite ores deposits are developed exclusively from the altered basalts [12]. Soils are dominated by ferralsols [17] associated with duricrusts which play an important role in the pedology of Adamawa region.

2.2. Sampling and Analytical Procedures

Based on the field relations and differences in duricrust facies, sixteen samples were collected (**Figure 3**). These were separated into two groups, the first referring to the samples from the trench's profiles and the second consisting of the blocks of duricrust outcropping on the ground surface. The first group included

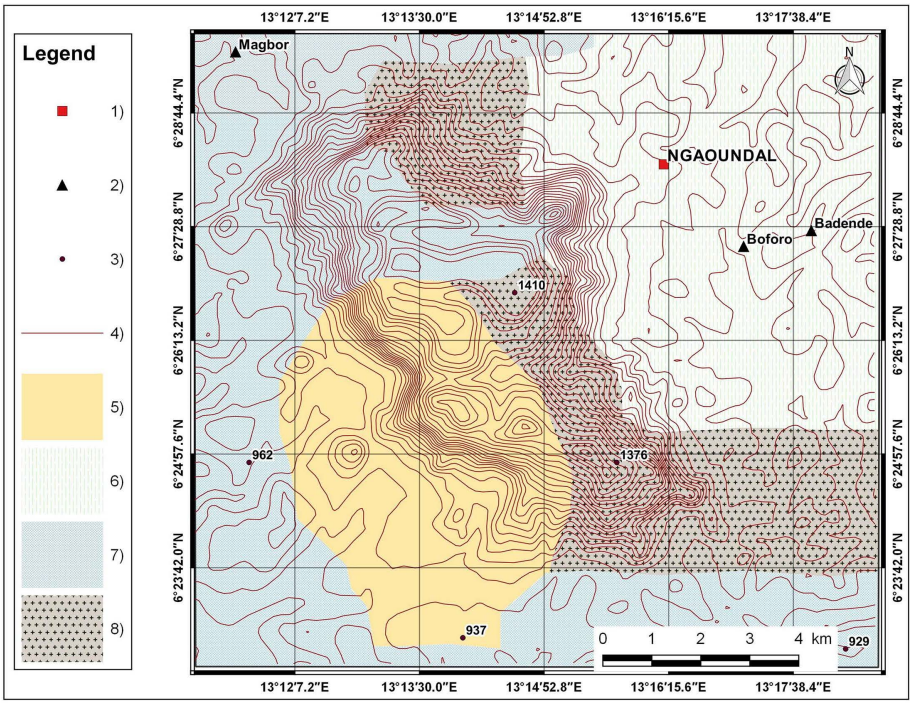

Figure 2. Geological map. 1) Ngaoundal Town, 2) locality, 3) rated point, 4) level curve, 5) bauxitic formations zone with alteration of basalts, 6) migmatites and various gneiss with some leptynites, quartzites, amphibolites and pyroxenites, 7) cretaceous, 8) old syntectonic massifs, essentially calco-alkaline granites.

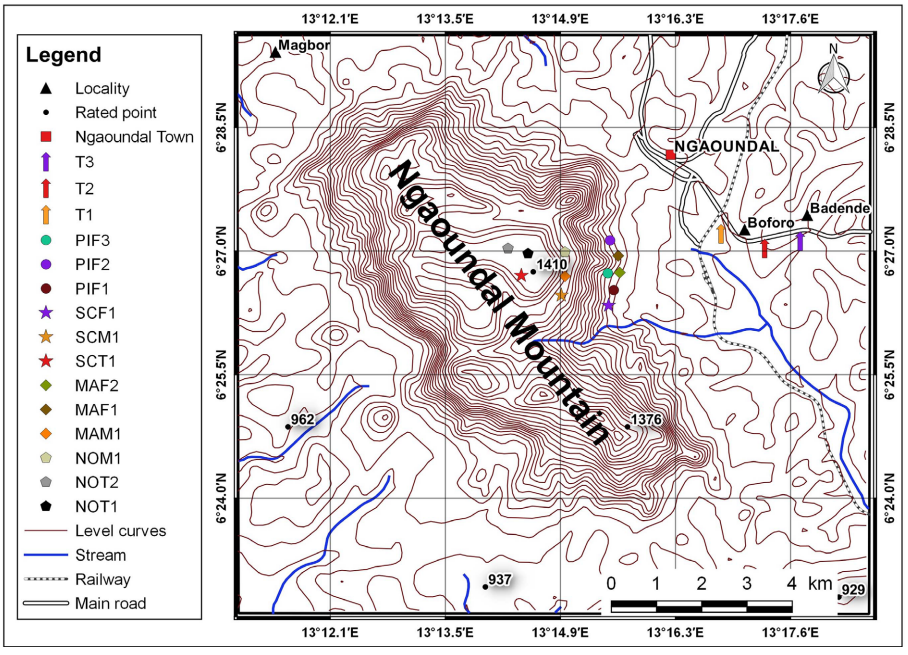

Figure 3. Sampling map of study area. T = Trench: profile obtained from trench road, PIF = Pisolitic facies collected at the foot of the hill, SCF = Scoriaceous facies collected at the foot of the hill, SCM = Scoriaceous facies collected at mid-slop, SCT = Scoriaceous facies collected at the top of the hill, MAF = Massive facies collected at the foot of the hill, MAM = Massive facies collected at mid-slop, NOM = Nodular facies collected at mid-slop, NOT = Nodular facies collected at the top of the hill.

four samples, two from the first profile and one from each of the last two. The second group was constituted of twelve samples classified into four facies (scoriaceous, pisolitic, massive and nodular), each with three samples. After morphological characterization, all sixteen samples were subjected to mineralogical and geochemical analysis at Geoscience Laboratories (Geo Labs) in Canada, after their preparation in the Mechanical Ore Preparation Laboratory of School of Mining, Industry and Geology of Niamey (Niger).

The mineralogical composition was semiquantitatively determined by using X-ray diffraction (XRD-100) after pulverizing sample powders with an agate mortar and pestle. Samples were analyzed with Co radiation at 40 kV and 45 mA. The following parameters were used in the X'PertHighScore Plus software for the peak identification, and a Rietveld Refinement process [18] was applied for semi-quantifying the proportion of each mineral.

The compositional values of major and minor oxides along with the trace and rare earth elements were determined by using X-Ray Fluorescence Spectrometry (WD-XRF) coupled to ICP-AES and ICP-MS methods. The LOI (Loss on ignition) values were measured on the basis of weighting the samples before and after one hour of heating at 1000˚C. The performance of each method employed at the Geo Labs is monitored using control charts of the analysis of interlaboratory and in-house reference materials. The overall precision of the analytical methods can be assessed from the reproducibility of the analyses of the reference materials that were cycled through as quality assurance monitors during sample analysis.

2.3. Data Analysis

The mobility of chemical elements during weathering was investigated using two indices of alteration, the Chemical Index of Alteration (CIA) and the Mineralogical Index of Alteration (MIA) [19]. The CIA evaluates cations (Ca^{2+}, Na^{+} and K^{+}) mobility in relation to Al^{3+} considered as immobile element while the MIA determines the degree of transformation of primary minerals into secondary minerals [20]. These indices are obtained by these formulae:

$\mathrm{CIA} = 100 \times \left[\dfrac{\mathrm{Al_2O_3}}{\mathrm{Al_2O_3} + \mathrm{CaO} + \mathrm{Na_2O} + \mathrm{K_2O}} \right]$. The MIA is deduced from the CIA formula: $\mathrm{MIA} = 2 \times (\mathrm{CIA} - 50)$. The obtained data were processed by using Excel program. The various diagrams were performed with Sigma Plot 14.5 while the various maps were generated using GOOGLE MAPS and QGIS version 2.18.15.

3. Results

3.1. Morphological Description

The morphological characterization of the duricrusts outcropping in blocks on the ground surface (**Figure 4**) showed that the scoriaceous facies (**Figure 4(a)**, **Figure 4(b)**, **Figure 4(c)**) was the most distributed. It was observed from the top to the bottom of the hill. It was mainly characterized by a mottled porous

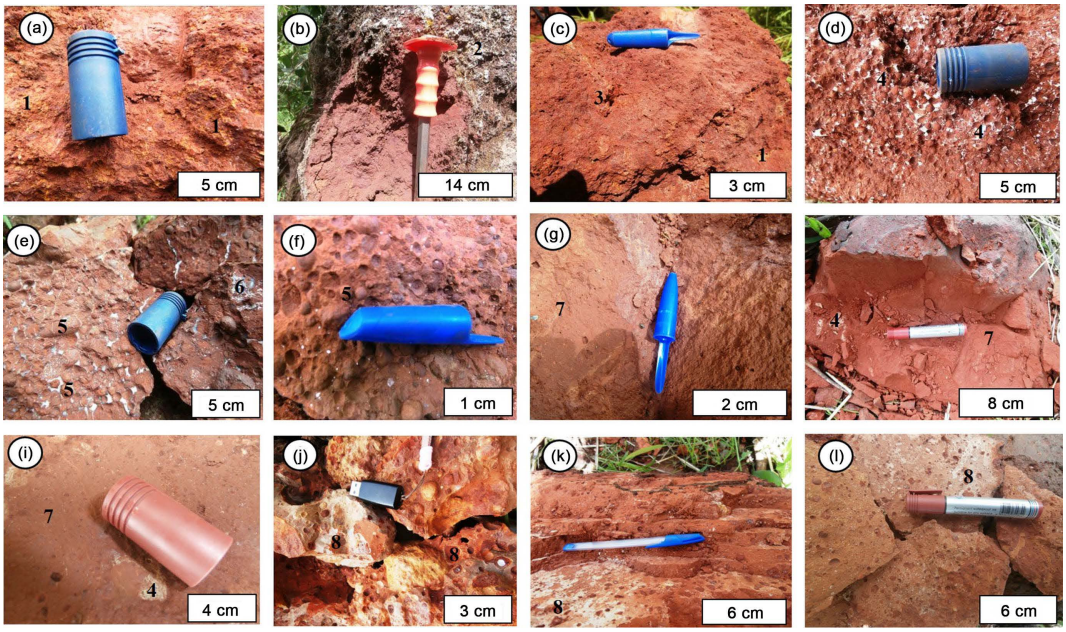

Figure 4. Different facies of the studied formations. (a)-(c) Scoriaceous facies re-spectively outcropping at the top, mid-slope and foot of the hill; (d)-(f) Nodular facies; (g)-(i) Massive facies; (j)-(l) Pisolitic facies. 1) yellowish stains, 2) Cortex, 3) marks of biological activities, 4) whitish stains, 5) nodules, 6) whitish bonds 7) red matrix, 8) pisoliths.

matrix; whose overall appearance gives them the character of a volcanic slag. The yellowish spots, which are very abundant in the summit formations (**Figure 4(a)**), tended to disappear in those of the mid-slop (**Figure 4(b)**) and the base of the hill (**Figure 4(c)**). The pisolitic facies (**Figures 4(j)-(l)**) was the least abundant and corresponded to the continuous bauxitic duricrusts which outcrop essentially at the foot of the hill. These formations were characterized by more or less friable spherical concretions contained in a red matrix. Massive and nodular facies outcropped at the top of the hill and at mid-slope. The former (**Figures 4(g)-(i)**) were very compact and very resistant. These were characterized by a nearly homogeneous red matrix and a total lack of nodules, but a few rare whitish spots within the matrix of the formations at the foot slope. The second ones (**Figures 4(d)-(f)**) presented red matrix containing millimeter to centimeter nodules in varying degrees of abundance. They also displayed white and gray punctuation on the formations of the top of the hill, while those of the mid-slope were stripped of the whitish spots.

Profiles description (**Figure 5**) focused on the variation in thickness of the horizons. It consists of: the structure or texture, color, traces of any biological activity, the limit between a layer and the one below, and the presence of vegetation cover.

The first profile (**Figure 5(a)**) with a thickness of 350 cm had three layers. The first (0 - 15 cm) was sandy-claybrown (7.5YR 4/3), rich in organic matter. It contained an abundance of fine roots and millimetric to centimetric nodules. Blocks of duricrust were found in outcropping. The limit with the underlying

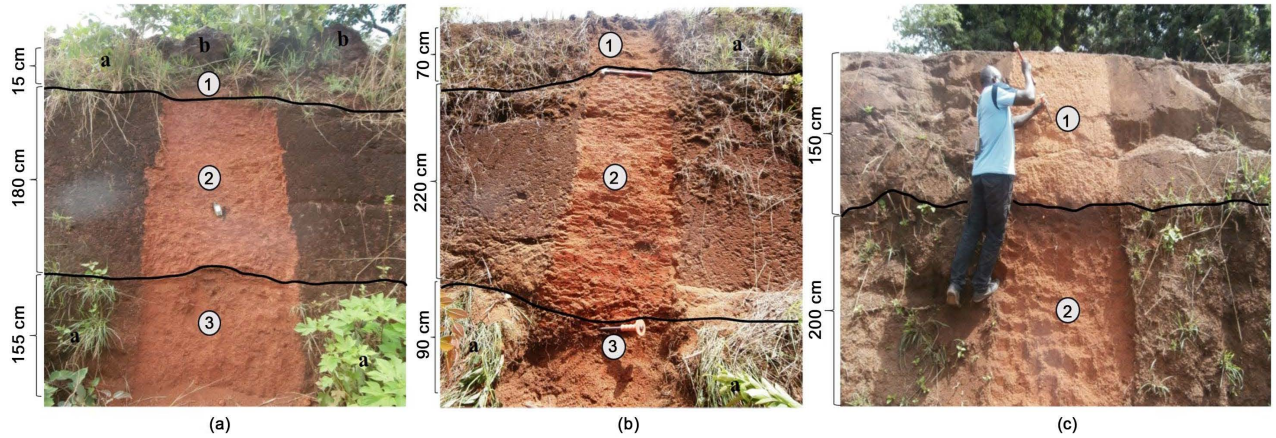

Figure 5. Profiles obtained from trench road. (a) First trench; (b) Second trench; (c) Third trench; a) Vegetation cover; b) Blocks of duricrust; 1) Upper layer; 2) Middle layer; 3) Lower layer.

level was clearly defined. The second level (15 - 195 cm) referred to a slab of reddish-brown duricrust (5YR 4/4), massive and compact. It showed relics of primary minerals and whitish spots. The transition was irregular throughout the trench and distinctive with the underlying level. The third and last horizon (195 - 350 cm) was marked by a yellowish-red clay layer (5YR 5/6), slightly compact and containing a high proportion of millimetric to centimetric nodules and abundant fine roots. It presented traces of biological activities and some relics of primary minerals.

The second profile (Figure 5(b)) was 380 cm in thickness and showed 3 layers. An upper level (0 - 70 cm) was brown nodular horizon (10YR 4/3). It enclosed fine roots and signs of biological activities. It contained millimetric to centimetric nodules. It presented clearly defined interface with the level below. An Intermediate level (70 - 290 cm) referred to slab of duricrust with a red background (2.5YR 4/6). It was very compact, very hard and contained very few fine roots, embedded in an abundance of rusty spots. Towards the transition to the bottom level, the matrix background changed to dark red. The limit was gradual with the inferior level. A lower layer (290 - 380 cm) was yellowish clayey red level (5YR 5/6), with a polyhedric structure and enclosing some rare fine roots, nodules and fragments of duricrust. It also included whitish patches disseminated within the complex.

The third and last profile (Figure 5(c)) was composed of 2 levels: the first one (0 - 150 cm) constituted of a dark brown duricrust (7.5YR 5/6), outcropped as a very compact and hard slab above loosen soils. A few rare vacuoles backfilled with dark brown soils were identified in a matrix that contained an abundance of rusty and whitish spots. The lower boundary was abrupt and regular. The second (150 - 350 cm) referred to red level (2.5YR 4/6), sandy-clay, containing many yellow spots and vacuoles filled with dark brown earth from biological activities. It contained fragments of duricrust, an abundance of fine roots and few yellowish spots.

3.2. Mineralogical Characterization

According to mineralogical analyses (Table 1), gibbsite was the most abundant mineral particularly in scoriaceous facies. It represented more than 90% of minerals detected by X-ray. Hematite is also recorded, but in low quantities (3.88% - 6.1%) whereas kaolinite, quartz and goethite were totally lack in these materials. In the pisolitic facies, mineral association included gibbsite, kaolinite, hematite and goethite. Kaolinite was the most abundant mineral in these facies. It represented 52.21% to 76.01% of minerals detected by X-ray. Gibbsite grade was fairly low, but a significant content in the PIF2 sample (25.93%) was observed. Similarly, hematite was weak but it was a quite high proportion in PIF3 sample (16.84%). The nodular facies were mostly composed of hematite (41.85% to 42.01%) and kaolinite (30.79% to 45.97%). The quartz content was moderate. It varied from 12.22% to 25.19%. There was a total lack of goethite and gibbsite minerals in these formations. Three minerals were distinguished in the massive red-bottom facies: gibbsite (19.73% to 59.43%), hematite (24.87% to 68.13%) and quartz (9.17% to 15.7%). The first two minerals (gibbsite and hematite) were the most abundant and quartz the least important.

The two lower layers of the first profile were examined. The upper level showed a significant proportion of quartz mineral (66.06%), a moderate content of gibbsite (24.84%) and a slight content of kaolinite (9.1 %). It did not include hematite and goethite. The lower layer indicated the same pattern with a content of 55.91% quartz, 34.02% gibbsite and 10.07% kaolinite and lack of hematite and goethite. The second profile analyzed on its second layer, displayed 78.39% gibbsite, 11% kaolinite and 10.61% quartz. These results confirmed a significant content of gibbsite. The third profile analyzed on its first level indicated an interested content of quartz (48.82%) and gibbsite (36.25%), and weaker in kaolinite (14.93%). Figure 6 shows the X-ray patterns of the analyzed samples.

3.3. Geochemical Features

3.3.1. Distribution of Major Elements

Major elements analyses (Table 2) indicated Al_2O_3, Fe_2O_3 and SiO_2 as the main oxides. Alkali (Na_2O, K_2O) and alkaline earth metals (MgO, CaO), along with P and Mn (as oxides) were present in rather low concentrations (sum of the average contents less than 1%).

Scoriaceous facies showed high concentrations of Al_2O_3. We noted 47.92% in the hilltop formations (SCT1), 45.57% in the mid-slope formations (SCM1) and 49.65%) in the foot of the hill formations (SCF1). Fe_2O_3 contents were lower. These were respectively 21.02% from SCT1, 24.19% from SCM1 and 17.9% from SCF1. TiO_2 was low (2.43%, 3.84% and 2.57% respectively) and silica in traces (< 1% in all the three samples). The pisolitic facies were mostly found at the foot of the hill. Three samples distinguished them: PIF1, PIF2 and PIF3. They showed interested concentrations of alumina (31.66%, 37.99% and 32.8% respectively) and silica (34.46%, 21.09% and 36.31%). Iron oxide was moderate (15.21%, 22.08% and 13.04%) and titanium oxide fairly low (3.81%, 4% and 4.11%). The

Table 1. Mineralogical composition (wt.%) obtained by quantitative Rietveld Refinement on the bauxitic duricrust. (-) = mineral absent or present but below calculation limits, *i.e.* <5%, SCT = Scoriaceous facies collected at the top of the hill, SCM = Scoriaceous facies collected at mid-slop, SCF = Scoriaceous facies collected at the foot of the hill, PIF = Pisolitic facies collected at the foot of the hill, NOT = Nodular facies collected at the top of the hill, NOM = Nodular facies collected at mid-slop, MAM = Massive facies collected at mid-slop, MAF = Massive facies collected at the foot of the hill, FTL2 = Level 2 of first trench, FTL3 = Level 3 from first trench, STL2 = Level 2 from second trench, TTL1 = Level 1 from third trench, T = Trench.

		Minerals content (wt.%)					
Facies/Profiles	**Samples**	**Kaolinite**	**Quartz**	**Goethite**	**Hematite**	**Gibbsite**	**Total**
Scoriaceous	SCT1	-	-	-	4.11	95.89	100
	SCM1	-	-	-	6.01	93.99	100
	SCF1	-	-	-	3.88	96.12	100
Pisolitic	PIF1	76.01	-	9.97	6.57	7.45	100
	PIF2	52.21	-	15.18	6.68	25.93	100
	PIF3	74.22	-	-	16.84	8.92	100
Nodular	NOT1	30.79	25.19	-	44.02	-	100
	NOT2	45.97	12.22	-	41.81	-	100
	NOM1	38.86	19.28	-	41.85	-	100
Massive	MAM1	-	15.7	-	24.87	59.43	100
	MAF1	-	12.14	-	68.13	19.73	100
	MAF2	-	9.17	-	41.18	49.65	100
T1	FTL2	9.1	66.06	-	-	24.84	100
	FTL3	10.07	55.91	-	-	34.02	100
T2	STL2	11	10.61	-	-	78.39	100
T3	TTL1	14.93	48.82	-	-	36.25	100

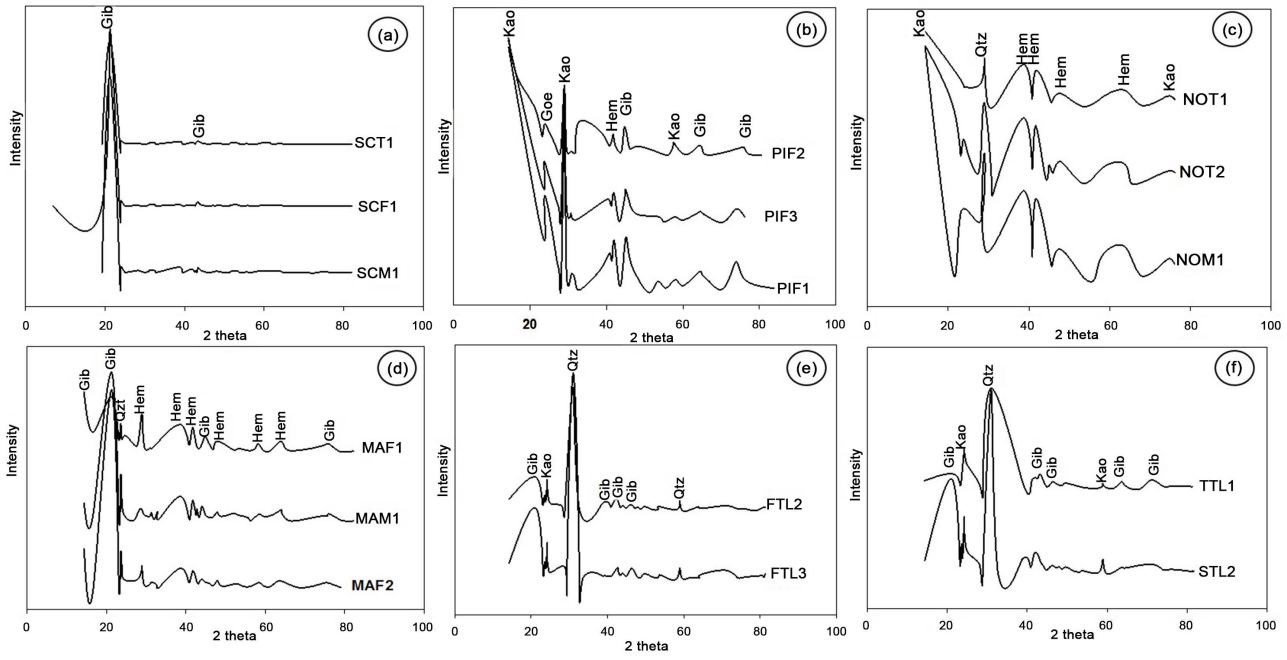

Figure 6. XRD patterns of the studied duricrust formations. (a) Scoriaceous facies (SCT1, SCM1 and SCF1), (b) Pisolitic facies (PIF1, PIF2 and PIF3), (c) Nodular facies (NOT1, NOT2 and NOM1), (d) Massive facies (MAF1, MAM1 and MAF2), (e) First trench (FTL2 and FTL3), (f) Second trench (STL2) and third trench (TTL1). Gib = Gibbsite, Kao = Kaolinite, Hem = Hematite, Goe = Geothite and Qzt = Quartz.

Table 2. Major elements (wt.%) of the studied bauxitic formation. LOI = Loss On Ignition; (D.L) = Detection Limits, SCT = Scoriaceous facies collected at the top of the hill, SCM = Scoriaceous facies collected at mid-slop, SCF = Scoriaceous facies collected at the foot of the hill, PIF = Pisolitic facies collected at the foot of the hill, NOT = Nodular facies collected at the top of the hill, NOM = Nodular facies collected at mid-slop, MAM = Massive facies collected at mid-slop, MAF = Massive facies collected at the foot of the hill, FTL2 = Level 2 of first trench, FTL3 = Level 3 from first trench, STL2 = Level 2 from second trench, TTL1 = Level 1 from third trench, T = Trench.

		Scoriaceous facies			Pisolitic facies			Nodular facies			Massive facies			T1		T2	T3
	D.L	**SCT1**	**SCM1**	**SCF1**	**PIF1**	**PIF2**	**PIF3**	**NOT1**	**NOT2**	**NOM1**	**MAM1**	**MAF1**	**MAF2**	**FTL2**	**FTL3**	**STL2**	**TTL1**
SiO_2	0.04	0.89	0.31	0.88	34.46	21.09	36.31	31.43	27.88	31.21	6.34	18.57	16.89	32.63	39.27	26.32	22.38
TiO_2	0.01	2.43	3.84	2.57	3.81	4	4.11	4.21	4.21	3.18	5.07	3.88	2.55	0.92	0.79	0.65	0.73
Al_2O_3	0.02	47.92	45.57	49.65	31.66	37.99	32.8	27.96	25.67	28.26	39.55	32.92	38.06	23.42	26.89	23.61	19.95
Fe_2O_3	0.01	21.02	24.19	17.9	15.21	22.08	13.04	22.53	30.15	23.54	27.33	29.72	21.34	24.12	15.92	31.43	39.46
MnO	0.002	0.023	0.063	0.062	0.02	0.028	0.028	0.028	0.025	0.032	0.023	0.031	0.029	0.027	0.017	0.023	0.025
MgO	0.01	0.03	0.04	0.08	0.07	0.04	0.1	0.11	0.1	0.08	0.06	0.08	0.04	0.11	0.08	0.11	0.1
CaO	0.006	0.025	0.014	0.015	0.054	0.035	0.055	0.025	0.042	0.031	0.024	0.042	0.012	0.032	0.014	0.01	0.026
Na_2O	0.02	0.04	0.04	0.05	0.05	0.04	0.05	0.03	0.03	0.03	0.03	0.03	0.03	0.03	0.04	0.02	0.02
K_2O	0.01	0.01	0.01	0.02	0.03	0.02	0.04	0.03	0.01	0.02	0.01	0.02	0.01	0.25	0.21	0.31	0.25
P_2O_5	0.002	0.113	0.089	0.134	0.102	0.162	0.112	0.062	0.213	0.112	0.134	0.194	0.093	0.108	0.025	0.128	0.298
LOI		26.65	25.08	27.62	13.64	14.29	13.27	12.62	11.08	12.68	20.18	14.24	19.37	17.53	15.52	16.88	15.66
Total		99.2	99.28	99.01	99.2	99.86	100.01	99.1	99.55	99.24	98.81	99.77	98.55	99.24	98.82	99.56	98.93
CIA		99.84	99.86	99.83	99.58	99.75	99.56	99.70	99.68	99.71	99.84	99.72	99.86	98.69	99.03	98.58	98.54
MIA		99.69	99.72	99.66	99.16	99.50	99.12	99.39	99.36	99.43	99.68	99.44	99.73	97.37	98.06	97.16	97.08

nodular facies were either enriched in alumina, or in iron oxides or silica. Indeed, NOT1 was more concentrated in silica (31.43%), then alumina (27.96%) and finally iron oxides (22.53%). In contrary, NOT2 was more focused in iron oxides (30.15%), followed by silica (27.88%) and alumina (25.65%). Titanium oxide, with a content of 4.21% in the two samples, was the least concentrated within these formations. The massive red-bottom facies were found at mid-slope (MAM1) and at the bottom of the slope (MAF1 and MAF2). They revealed significant alumina concentrations. Indeed, the first ones showed a content of 39.55%, the second ones of 32.92% and the third ones of 38.06%. They enclosed respective contents of iron oxides of 27.3%, 29.72% and 21.34%. Silica was showed in respective proportions of 6.34%, 18.57% and 16.89%. Titanium oxide was less concentrated (5.07%, 3.88% and 2.55% respectively in MAM1, MAF1 and MAF2).

The geochemistry of major elements along the profiles indicated that their proportions varied from one layer to another. The first profile indicated significant silica levels in the two samples constituted: 32.63% from FTL2 and 39.27% from FTL3. Alumina concentration ranged from 23.42% to 26.89% and iron oxide from 15.92% to 24.12%. Titanium oxide was encountered in trace amounts

(<1%). Geochemical analysis of the second profile (STL2) revealed significant proportions of iron oxides (31.43%). Silica and alumina contents were respectively 26.32% and 23.61%. Titanium oxide was weak (0.65%). On geochemical point of view, third profile (TTL1) analysis showed a most abundant content of iron oxides (39.46%), followed by silica (22.38%) and alumina (19.95%). Titanium oxide was weak (0.73%). The Chemical Index of Alteration (CIA) and the Mineralogical Index of Alteration (MIA) shown in Table 2 were very high (>99%).

3.3.2. Behavior of Trace Elements

Trace element analyses (Table 3) generally revealed low values of various elements. However, there was a certain number of variations in content from one facies to another one. This is the case of Zr, Cr and V on one hand and Ba, Ga, Nb and Pb on the other hand. In Scoriaceous facies, Zr, Cr and V contents ranged from 189 to 337 ppm; Ba, Ga, Nb and Pb from 22.58 to 134.5 ppm, with a more significant proportion of Ba (134.5 ppm) in the formation outcropped at the foot of the hill (SCF1). Except V, which is totally lack, trace elements were generally well distributed in the pisolitic facies. The values ranged from 396 to 427 ppm in the case of Zr and from 510 to 744 ppm in the case of Cr. Ba was fairly low (8.7 to 21.7 ppm) whereas Ga and Nb as well as Ni display average proportions exceeding 50 ppm with maxima in Ni (118.1 ppm) in PIF1 sample. Nodular duricrusts generally displayed significant concentrations in Zr and Cr. These levels were more or less important in summit formations (NOT1 and NOT2) than those of mid-slope (NOM1). The values ranged from 344 to 785 ppm for Cr and from 260 to 346 ppm for Zr. V, while lacking in NOT2, is more than 250 ppm in the two other samples. Ba was very concentrated (111.9 ppm) in NOT2. Ga, Nb and Ni presented values greater than 30 ppm. Zr was more concentrated (473 ppm) in the mid-slope massive facies (NOM1) than those of the foot of the slope (236 and 362 ppm). Furthermore, the greatest Cr content was observed in the bottom of the slope formations, namely in the MAF2 sample (809 ppm), which was totally lacking in V. Ga, N and Ni were moderate (an average content of more than 40 ppm) while Ba was weakest (average content less than 20 ppm).

Concerning profiles, a similar trend was observed. The first profile indicated an average of more or less 300 ppm of Zr, Cr and V (Table 3). These decreased from the top to the bottom level, as well as Ba, Ga and Nb, which increased between 20 and 40 ppm. Ni increased as depth increases with 380.5 ppm in the sample from the bottom level. Cr was the most enriched element (391 ppm) in STL2, followed by V (370 ppm) and Zr (215 ppm) respectively. The other trace elements (Ba, Ga, Nb and Ni) were moderate (17.21 to 32.25ppm) but Ni and Ba were significantly more enriched (71.3 and 65.1 ppm respectively). According to TTL1 sample, V was the most reported trace element (370 ppm) near Cr (208 ppm) and Zr (198 ppm). Ba and Ni were fairly moderate (48.6 and 54.6 ppm respectively), but Ga and Nb were quite weak (23.53 and 18.18 ppm respectively).

Table 3. Trace elements content (ppm) of the studied formations. (-) = Not detected or below the Detection Limit (D.L), SCT = Scoriaceous facies collected at the top of the hill, SCM = Scoriaceous facies collected at mid-slop, SCF = Scoriaceous facies collected at the foot of the hill, PIF = Pisolitic facies collected at the foot of the hill, NOT = Nodular facies collected at the top of the hill, NOM = Nodular facies collected at mid-slop, MAM = Massive facies collected at mid-slop, MAF = Massive facies collected at the foot of the hill, FTL2 = Level 2 of first trench, FTL3 = Level 3 from first trench, STL2 = Level 2 from second trench, TTL1 = Level 1 from third trench, T = Trench.

		Scoriaceous facies			Pisolitic facies			Nodular facies			Massive facies			T1		T2	T3
	D.L	**SCT1**	**SCM1**	**SCF1**	**PIF1**	**PIF2**	**PIF3**	**NOT1**	**NOT2**	**NOM1**	**MAM1**	**MAF1**	**MAF2**	**FTL2**	**FTL3**	**STL2**	**TTL1**
Ba	0.8	60.8	71.9	134.5	21.7	8.7	14.1	8.2	111.9	16.9	5.7	13	25.2	39.9	25.7	65.1	48.6
Be	0.04	0.17	0.23	0.43	1.38	2.27	0.85	0.14	0.36	0.57	0.33	1.2	0.43	1.39	1.06	1.14	2.36
Cr	3	297	266	189	744	510	590	434	785	344	382	283	809	365	143	391	208
Cu	1.4	5.1	6.9	13.2	17.3	29	23.6	5.5	9.4	39.3	11	17.4	15.5	23.9	25	26	29.7
Ga	0.04	41.14	51.66	29.9	55.63	>58	39.3	36.61	40.54	34.93	50.35	44.17	44.22	36.35	35.85	32.25	29.53
Hf	0.14	8.94	8.96	5.35	10.43	11.25	10.15	9.19	8.72	6.61	11.78	8.91	6.52	9.58	9.17	5.82	5.37
Li	0.4	0.6	<0.4	<0.4	8.6	10.1	3	2	3.7	5.9	0.8	3.6	3.9	11.1	10.7	6.3	15.9
Mo	0.08	3.61	3.49	2.43	2.23	5.96	1.79	2.19	3.9	1.87	3.99	4.8	6.83	16.39	12.16	7.48	8.83
Nb	0.028	47.25	54.34	28.82	53.77	53.69	54.11	47.35	45.26	31.09	61.20	47.78	24.20	26.49	23.15	17.21	18.18
Nd	0.06	9.1	56	16.07	2.44	2.24	8.66	13.98	101.37	13.99	1.54	3.62	90.75	12.74	8.86	30.27	27.96
Ni	0.7	8.6	6.4	16.9	118.1	77	63.3	19.4	87.8	79.9	20.4	47.5	61.9	69.4	380.5	71.3	54.6
Pb	0.18	21.85	22.58	35.39	7.14	10.8	6	14.91	24.4	11.67	9.06	8.65	44.31	31.8	25.22	38.67	45.79
Rb	0.11	0.6	0.89	1.95	1.46	1.34	1.68	1.16	1.62	1.82	1.31	1.1	1.31	28.91	20.6	26.14	21.43
Sb	0.04	0.58	0.37	0.26	0.2	0.25	0.14	0.17	0.22	0.1	0.29	0.19	0.23	1.12	0.45	1.17	1.41
Sc	1.1	13.2	10.8	13.9	38.8	39.5	35.8	21.4	28.6	33.6	32	38.1	20.1	15.9	13.8	17.2	21.6
Sn	0.16	3.4	4.02	2.52	5.25	5.51	4.66	3.33	3.66	2.96	5.03	3.77	2.81	3.28	3.21	2.44	2.32
Sr	0.6	47.1	34.3	57.1	6.2	5	7.7	7.6	167.1	28.3	2.3	7.2	24.4	11.5	7.5	23.2	14.7
Ta	0.007	3.073	3.42	1.789	3.432	3.521	3.491	2.961	2.754	1.924	3.731	2.921	1.561	1.983	1.912	1.244	1.297
U	0.011	1.72	1.414	1.456	3.183	2.59	1.452	1.259	1.959	1.005	2.81	2.254	3.565	10.526	12.745	8.572	12.227
V	0.8	255.3	316.5	248.1				281.2		266.4	>370	>370		356.8	211.4	>370	>370
Zn	1.8	9.8	15.8	22.3	34.8	25.5	42.9	15.5	52.4	23.5	4.7	21.4	21.8	17.6	12.1	16.2	11.7
Zr	6	337	340	202	405	427	396	360	346	260	473	362	236	352	327	215	198

3.4. Relationship among Chemical Components

Chemical elements may have certain relationships during the bauxitization process. Binary plots among the major elements indicate strongly positive correlations between Fe_2O_3 and P_2O_5; Al_2O_3 and TiO_2; Nb and TiO_2; Ta and TiO_2 (Figure 7). A moderate positive correlation is observed between Fe_2O_3 and MgO whereas negative correlations exist between Al_2O_3 and SiO_2, and Al_2O_3 and Fe_2O_3. These patterns suggest two groups of components: a first group of positively correlated components including Al_2O_3 vs. TiO_2 diagram (Figure 7(f)), Fe_2O_3 vs. P_2O_5 (Figure 7(e)), Fe_2O_3 vs. MgO (Figure 7(d)), Nb vs. TiO_2 (Figure 7(h)) and Ta vs. TiO_2 (Figure 7(i)) and a second group of negatively associated components composed of Fe_2O_3 vs. Al_2O_3 diagram (Figure 7(a)), Fe_2O_3 vs. SiO_2 (Figure 7(b)), Al_2O_3 vs. SiO_2 (Figure 7(c)) and Al_2O_3 vs. Cr (Figure 7(g)).

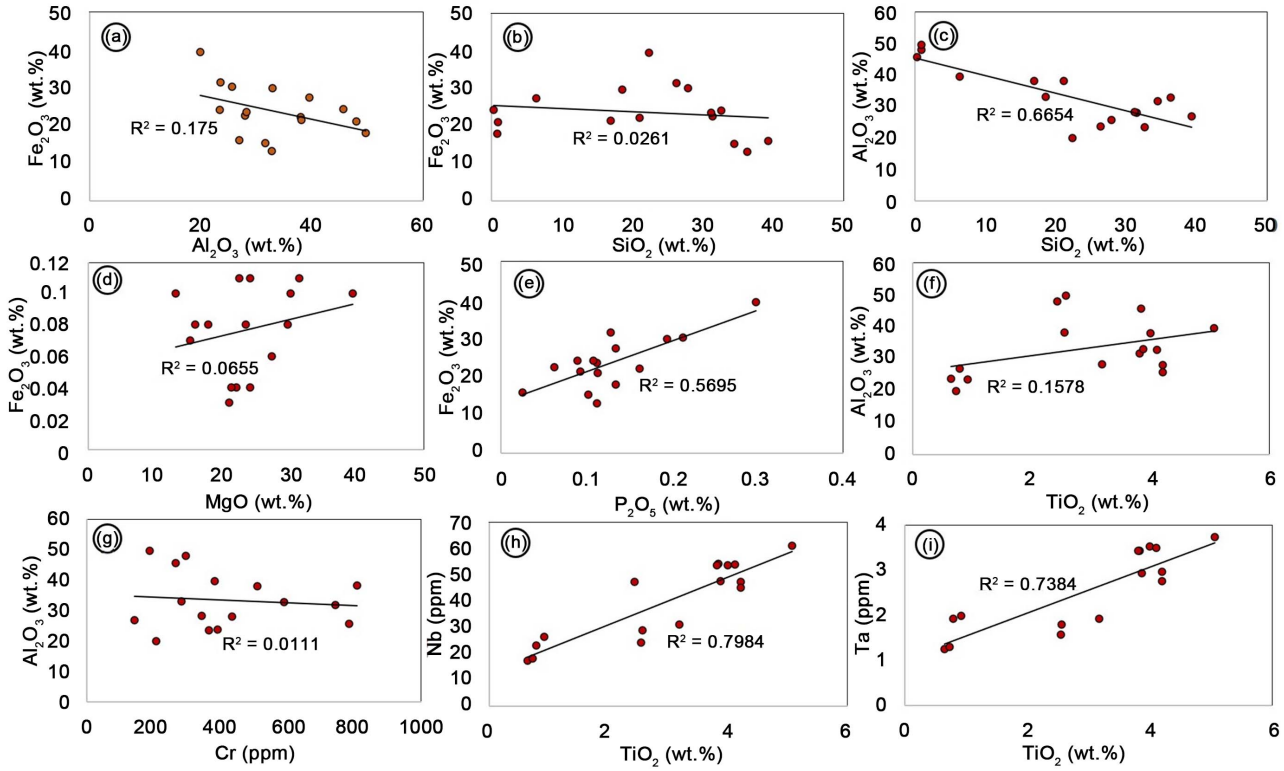

Figure 7. Binary plots and R values showing the correlation between certain oxides (expressed in wt.%) and the trace elements (expressed in ppm). (a) Fe_2O_3 vs. Al_2O_3; (b) Fe_2O_3 vs. SiO_2; (c) Al_2O_3 vs. SiO_2; (d) Fe_2O_3 vs. MgO; (e) Fe_2O_3vs. P_2O_5; (f) Al_2O_3 vs. TiO_2; (g) Al_2O_3 vs Cr; (h) Nb vs. TiO_2; (i) Ta vs. TiO_2.

4. Discussion

4.1. Variation of Bauxitic Duricrust Facies

Weathering of basalts developed during the upper Cretaceous was the origin of concentrated bauxite deposits on the platform of Ngaoundal and Minim-Martap in the Adamawa Region of Cameroon [7] [8] [9] [12]. Morphological facies variation (scoriaceous, nodular, pisolitic and massive) corroborate with the fact that these materials are derived from the erosion and re-sedimentation of older formations and possibly also from eroded bauxitic formations, formed on the exposed platform [6]. This degradation process was favored by humid equatorial climate [21] and tectonic instability [22] of the region which belongs to the Cameroon volcanic line. According to [4] and [23], the African morphologies depend on the progressive erosion and peneplanation which are favored by the hydrographic network which generally get along with the faults and are responsible for the reduction and variations of the thickness of the duricrust formations above the plateaus and on the flanks of hills. The white and gray punctuation displayed by certain bauxitic facies would result from the weathering of plagioclases, substituted in volume and form by gibbsite and ferruginous minerals [6] [12]. The transformation of the bauxitic formations into the pisolitic bauxitic facies by individualisation of pisoliths derived from ferruginous spots and nodules, led to the development of a thick bauxitic mantle with pisolitic facies [12] [24].

The landscape and the pedological coverage of the study area reveal that the hills are very narrow with very steep slopes, unlike the plateaus where the slopes are slightly inclined [6] [12]. The presence of the gibbsitic-dominated duricrust has contributed to the development of a thick soil-cover at the level of the hills, a compact pedologic horizon at the top of the plateaus and in the whole of a spotted horizon rich in quartz reflect the climatic contrast of the locality [5] [9].

4.2. Mineralogical and Geochemical Transformations

Bauxitic mantles that are regularly located at the top of hills and interfluves in the Ngaoundal area constitute a residual surface dominated by duricrust formations. These were probably formed during the upper Cretaceous under contrasted climate in an oxidizing-leaching environment that favored the crystallization of hematite more than goethite [25] [26]. The sustained presence of hematite mainly in the nodular and massive duricrust facies implies neutral to sligthly alkaline conditions in a later stage of bauxite formation. Moreover, its presence implies epigenetic processes during bauxitization, including Fe-mobilization, Fe-reprecipitation as amorphous Fe-hydroxides and subsequent recrystallization to hematite during diagenesis. In this context, hematite was shown to form contemporaneously to Al-oxyhydroxides [27]. The residual phase of the altered basalt cover included iron hydroxides (hematite, goethite), clay minerals, kaolinite and a considerable volume of aluminium-free hydroxides [12]. Thus, lateritization in Ngaoundal favored bauxitization through aluminium mobilization with individualization of the iron bearing lateritic bauxites which develop thick bauxitic mantles [8]. This suggests that bauxitization in this environment may correspond to intense hydrolysis leading to allitization with losses of SiO_2 and various cations, and monosialitization leading to the formation of kaolinite [28]. This intense weathering leads to the accumulation of significant immobile elements as Al, Fe and Si.

Climate conditions during bauxitic formations control the distribution of chemical elements between textural components [29]. For the major elements, we found the usual pattern of lateritic weathering [21]: progressive silica leaching, almost total alkali and alkaline earths leaching, gradual accumulation of iron and aluminum. Some elements are mostly concentrated in the matrix while other elements are associated with the ooids. This is the case of SiO_2 which is generally confined in the matrix, whereas Al_2O_3, TiO_2, and Fe_2O_3 are mostly associated with the ooids [30] [31]. However, the SiO_2 enrichment of the Sardinia bauxites is considered to be due to the alteration process caused by the circulation of Si-rich solutions, which caused the re-silicification of hematite as a consequence of the emplacement of Tertiary volcanites on top of the bauxites [28]. Relatively high iron contents (average value of 23%) indicate that these belong to iron-rich bauxites. Thus, the Ngaoundal bauxite deposits can be classified as ferruginous lateritic bauxites [32]. The most abundant trace elements (Zr, Cr and V), represent the elements that are not very mobile during alteration, and are most often enriched in bauxites [29].

In these formations, some correlations between major and trace elements were noted. Thus, a significantly negative correlation was observed in Al_2O_3 vs. SiO_2 diagrams (r = 0.815) and slightly negative between Fe_2O_3 and Al_2O_3 (r = 0.418). On the other hand, the correlation was significantly positive for Fe_2O_3 and P_2O_5 (r = 0.754); Nb and TiO_2 (r = 0.893) and Ta and TiO_2 (r = 0.830). Similarly, it was also positive for Fe_2O_3 and MgO (r = 0.504) and Al_2O_3 and TiO_2 (r = 0.830), but not significant. During the bauxitization process, a fractionation of major, minor and trace elements takes place [31]. It is widely accepted that the study of immobile elements is a powerful tool to unravel the parental material and the genetic history of bauxites [33]. Therefore, an identification of mobile and immobile elements during the bauxitization process is of vital importance. Furthermore, it has been shown that titanium oxides in bauxite can accumulate substantial amounts of Nb, Ta, Th [34]. In this study, the observed positive correlation between TiO_2 and Al_2O_3 might be attributed to the fact that Al-oxyhydroxides have been found to contain Ti-nanominerals [27]. Trace elements, such as Nb, Ta, Zr, Th or U show a good correlation with TiO_2 and Al_2O_3, meaning that they also behaved rather immobile during bauxitization. The good correlation between Nb and Ta with TiO_2 indicate that these elements are hosted in Ti-oxide phases within bauxitic samples. These correlations are typical of strongly weathered deposits where immobile elements accumulate and mobile elements are leached out [35]. This is also confirmed by the low contents of alkali and alkaline earth metals, which are highly mobile during chemical weathering [36] [37].

4.3. Weathering Level of the Studied Materials

Allitization, which refers to lateritization process, may be related to abundant rainfall (around 1500 to 1700 mm mean annual rainfall), dense and dendritic hydrographic network and steep slopes which favored a highly leaching milieu [38]. Bauxitization process of Ngaoundal duricrust formations was implemented by factors such as deferrugenization-ferrugenization, desilisification, and fluctuation of underground water table level. Chemical Index of Alteration (CIA) and Mineralogical Index of Alteration (MIA) derived from major element composition of the studied bauxites, showed extremely high values (>99). This is caused by the intense weathering resulted from high temperature, rainfall and regional groundwater system in the region [39]. The consequence is almost total exportation of alkali and alkaline earths elements (Na, Ca, Mg, K) and the accumulation of an important aluminum enrichment as well as abundant accumulation of gibbsite.

4.4. Implication of the Study on Mining Perspectives

The Cameroonian territory is full of more than fifty mineral substances and about 50% of the national territory has been explored. Between 1960 and 1990, the government with their international partners like UNDP and BRGM carried out studies in order to investigate the mineral potential of the country [40]. No-

wadays, the government through their development strategy (SND30), oriented projects on mining. This is emphasized by the creation of SONAMINES which is in charge of mining exploitation. But at first, the need of understanding processes which control establishment of minerals and relationship with environment are important for sustainable management.

The geology of Cameroon is favorable to the mineralization of substances as precious metals, base metals and rare metals [12]. Indeed, in Cameroon, lateritic weathering and erosion concentrated both metallic and non-metallic ores, as well as valuable substances, of which main indices and deposits have been identified. This is the case of bauxite deposits from Ngaoundal and Minim Martap in Adamawa [8] [12] and from FongoTongo in the Western region [6]. For example, 554 million tons of bauxite reserves have been found in the Adamawa region as of 2009 and 50 million tons in FongoTongo and 4 million tons in Foumban [8]. According to experts, Cameroon is the second largest bauxite reserves deposit in Africa.

Duricrusts described indicated the successive steps in the establishment of the bauxitic formations in Cameroon in general and in the Adamawa region in particular. The alteration of basaltic rocks of the Adamawa Plateau resulted in the deposit of alumina-rich bauxites in the high landscapes notably those of Ngaoundal [7] [12]. The study revealed interesting bauxite deposits in Ngaoundal area, thereby allowing the mining properties of the studied formations to be established. Indeed, significant concentrations of Al_2O_3 (over 45% in grade) on the one hand, and gibbsite (more than 90% in grade) on the other hand, notably in the most abundant scoriaceous duricrust facies in this area, sufficiently indicate favorable mining perspectives. The mineralogical and geochemical investigations conducted in this study allowed for a better assessment of industrial and technological properties of the bauxitic formations developed [33] [41]. However, further investigations including drillings and prospecting wells are required for establishing the geologic properties of deposit.

5. Conclusions

This study aimed to assess the behavior and the distribution of major and trace elements within studied formations in evaluating their mining potential. It should be noted that the study highlighted some points to be retained:

Four main facies of duricrust were identified and characterized: scoriaceous, pisolitic, nodular and vacuolar. They outcropped in blocks, from the top to the bottom of the hill, but the scoriaceous facies was the most widespread. The weathered profiles described enclosed in their various layers, slabs of duricrust with properties similar to those of the other layers.

After analytical procedures, it can be concluded that geochemical analyses revealed significant contents of Al_2O_3 notably in the scoriaceous facies, Fe_2O_3 and SiO_2, limited quantities of alkalis (Na_2O, K_2O) and alkaline earths metals (MgO, CaO) and low values of trace elements. Mineralogical investigations showed very high concentrations of gibbsite mainly in the scoriaceous facies, good contents

of kaolinite and moderate proportions of hematite. Allitization and monosiallitization are the two crystallochemical phenomena responsible for mineral development during weathering of the studied duricrust.

The study showed a mining interest of bauxitic duricrust, although it needs to be supplemented by further investigations based on the establishment of ore deposits and sampling in other localities where outcrops have been observed. This would enable us to establish a sufficient database to better understand the mining potential of the Ngaoundal area. It can therefore be concluded that the bauxitic mantles in Ngaoundal and surroundings, through their distribution in the landscape, their vertical organization and the evolution of bauxitic facies, contributed significantly to the overall levelling of the Adamawa plateau.

Conflicts of Interest

The authors declare no conflicts of interest regarding the publication of this paper.

References

[1] Liu, X., Wang, Q.F., Deng, J., Zhang, Q., Sun, S. and Meng, J. (2010) Mineralogical and Geochemical Investigations of the Dajia Salento-Type Bauxite Deposits, Western Guangxi, China. *Journal of Geochemical Exploration*, **105**, 137-152. https://doi.org/10.1016/j.gexplo.2010.04.012

[2] Meyer, F.M. (2004) Availability of Bauxite Reserves. *Natural Resources Research*, **13**, 161-172. https://doi.org/10.1023/B:NARR.0000046918.50121.2e

[3] Abedini, A. and Calagari, A.A. (2014) REE Geochemical Characteristics of Titanium-Rich Bauxites: The Permian Kanigorgeh Horizon, NW Iran. *Turkish Journal of Earth Sciences*, **23**, 513-532. https://doi.org/10.3906/yer-1404-11

[4] Temgoua, E., Bitom, D., Bilong, P., Lucas, Y. and Pfeifer, H.R. (2002) Démantèlement des Paysages Cuirassés Anciens en Zones Forestières Tropicales d'Afrique Centrale: Formation des Accumulations Ferrugineuses Actuelles en Bas de Versants. *Compte Rendu Géoscience*, **334**, 537-543. https://doi.org/10.1016/S1631-0713(02)01793-5

[5] Bitom, D.L., Volkoff, B., Beauvais, A., Seyler, F. and Ndjigui, P.D. (2004) Rôle des héritages latéritiques et du niveau des nappes dans l'évolution des modelés et des sols en zone intertropicale forestière humide. *Comptes Rendus Geoscience*, **336**, 1161-1170. https://doi.org/10.1016/j.crte.2004.03.019

[6] Momo, N.M., Beauvais, A., Tematio, P., Ambrosi, J.-P., Yemefack, M., *et al.* (2019) Lateritic Weathering of Trachyte, and Bauxite Formation in West Cameroon: Morphological and Geochemical Evolution. J*ournal of Geochemical Exploration*, **205**, Article 106324. https://doi.org/10.1016/j.gexplo.2019.06.006

[7] Sini, A., Basga, S.D., Temga, J.P. and Nguetnkam, J.P. (2020) The Influence of Topography in Duricrust Development in the Ngaoundal-Dir Section of Central Cameroon: Understanding Morphological, Mineralogical and Geochemical Transformations. *Scientific African*, **10**, e00655. https://doi.org/10.1016/j.sciaf.2020.e00655

[8] Tchamba, A.B., Yongue, R., Melo, U.C., Kamseu, E., Njoya, D. and Njopwouo, D. (2008) Caractérisation de la bauxite de Haléo Danielle (Minim-Martap, Cameroun) en vue de son utilisation industrielle dans les matériaux à haute teneur en alumine. *Silicates Industriels*, **73**, 77-84.

[9] Sojien, T.M., Mamdem, T.E.L., Wouatong, L.S.A. and Bitom, D.L. (2018) Mineralogical, Goechemical and Distribution Study of Bauxites in the Locality of Bangam and Environs (West Cameroun). *Earth Sciences Research*, **7**, 117-130. https://doi.org/10.5539/esr.v7n1p117

[10] Tchotsoua, M., Esoh, E., Mohamadou, G. and Ngana, J.-P. (1998) Diagnostic de l'état de l'environnement de Ngaoundéré et contribution pour une approche de gestion. *Annales de la FALSH*, **3**, 99-144.

[11] Yonkeu, S. (1993) Végétation des pâturages de l'Adamaoua (Cameroun): Ecologie et potentialités pastorales. Thèse de Doctorat, Université de Renne I, N° d'ordre 863, 213 p.

[12] Eno Belinga, S.M. (1972) Altération des roches basaltiques et le processus de bauxitisation dans l'Adamaoua (Cameroun). Thèse, Université Paris VI, Paris, 26-31.

[13] Njanko, T., Nédélec, A. and Affaton, P. (2006) Synkematic High-K Calc-Alkaline Plutons Associated with the Pan-African Central Cameroon Shear Zone (W-Tibati Area): Petrology and Geodynamic Significance. *Journal of African Earth Sciences*, **44**, 494-510. https://doi.org/10.1016/j.jafrearsci.2005.11.016

[14] Ganwa, A.A., Siebel, W., Frisch, W., Shang, C.K. and Ekodeck, G.E. (2011) Geochemistry and Geochronology of the Méigangametadiorite: Implications on the Timing of D2 Deformational Phase in Adamawa Yadé Domain in Cameroon. *International Journal of Biological and Chemical Sciences*, **5**, 1754-1767. https://doi.org/10.4314/ijbcs.v5i4.37

[15] Dawaï, D., Tchameni, R., Bascou, J., Awe, W.S., FossoTchunte, P.M. and Bouchez, J.L. (2017) Microstructures and Magnetic Fabrics of the Ngaoundere Granite Pluton (Cameroon): Implications to the Late-Pan-African Evolution of Central Cameroon Shear Zone. *Journal of African Earth Sciences*, **129**, 887-897. https://doi.org/10.1016/j.jafrearsci.2017.02.027

[16] Nkouandou, O.F., Ngounouno, I. and Deruelle, B. (2010) Géochimie des laves basaltiques récentes des zones Nord et Est de Ngaoundéré (Cameroun, Plateau de l'Adamaoua, Afrique centrale): Pétrogenèse et nature de la source. *International Journal of Biological and Chemical Sciences*, **4**, 984-1003. https://doi.org/10.4314/ijbcs.v4i4.63038

[17] WRB (2014) World Reference Base for Soil Resources. International Soil Classification System for Naming Soils and Creating Legends for Soil Maps. World Soil Resources Reports No. 106, FAO. (Update 2015)

[18] Ufer, K., Stanjek, H., Roth, G., Dohrmann, R., Kleeberg, R. and Kaufhold, S. (2008) Quantitive Phase Analysis of Bentonites by the Rietveld Method. *Clays and Clay Minerals*, **56**, 272-282. https://doi.org/10.1346/CCMN.2008.0560210

[19] Nesbitt, H.W. and Young, G.M. (1982) Early Proterozoic Climates and Plate Motions Inferred from Major Element Chemistry of Lutites. *Nature*, **299**, 715-717. https://doi.org/10.1038/299715a0

[20] Price Jason, R. and VelbelMichael, A. (2003) Chemical Weathering Indices Applied to Weathering Profiles Developed on Heterogeneous Felsic Metamorphic Parent Rocks. *Chemical Geology*, **202**, 397-416. https://doi.org/10.1016/j.chemgeo.2002.11.001

[21] Tardy, Y., Melfi, A.J. and Valeton, I. (1988) Climats et Paléo-climats Tropicaux Péri Atlantiques. Rôle des Facteurs Climatiques et Thermodynamiques (Température et Activité de l'Eau) sur la Répartition et la Composition Minéralogique des Bauxites et des Cuirasses Ferrugineuses au Brésil et en Afrique. *Comptes Rendus de l'Académie des Sciences*, **306**, 289-295.

[22] Valeton, I. and Melfi, A.J. (1988) Distribution Pattern of Bauxites in Cataguases Area (SE Brazil) in Relation to Lower Tertiary Paleogeography and Younger Tectonics. *Sciences Géologiques, Bulletins et Mémoires*, **41**, 85-98. https://doi.org/10.3406/sgeol.1988.1783

[23] Nono, A., Likeng, J.D.H., Wabo, H., Tabue Youmbi, G. and Biaya, S. (2009) Influence de la nature lithologique et des structures géologiques sur la qualité et la dynamique des eaux souterraines dans les hauts plateaux de l'Ouest-Cameroun. *International Journal of Biological and Chemical Sciences*, **3**, 218-239. https://doi.org/10.4314/ijbcs.v3i2.44516

[24] Churchman, G.J. (2000) The Alteration and Formation of Soil Minerals by Weathering. In: Sumner, M.E., Ed., *Handbook of Soil Science*, CRC Press, Boca Raton, 3-76.

[25] Beauvais, A. and Tardy, Y. (1993) Degradation and Dismantling of Iron Crust under Climatic Changes in Central Africa. *Chemical Geology*, **107**, 277-280. https://doi.org/10.1016/0009-2541(93)90190-T

[26] Tardy, Y. and Nahon, D. (1985) Geochemistry of Laterites Stability of Al-Goethite, Al-Hematite and Fe-Kaolinite in Bauxites and Ferricretes: An Approach to of Concretion Formation. *American Journal Sciences*, **285**, 865-903. https://doi.org/10.2475/ajs.285.10.865

[27] Gamaletsos, P.N., Godelitsas, A., Kasama, T., Church, N.S., Douvalis, A.P., Göttlicher, J., Steininger, R., Boubnov, A., Pontikes, Y., Tzamos, E., *et al.* (2017) Nano-Mineralogy and -Geochemistry of High-Grade Diasporic Karst-Type Bauxite from Parnassos-Ghiona Mines, Greece. *Ore Geology Reviews*, **84**, 228-244. https://doi.org/10.1016/j.oregeorev.2016.11.009

[28] Certini, G., Wilson, M.J., Hillier, S.J., Fraser, A.R. and Delbos, E. (2006) Mineral Weathering in Trachydacitic-Derived Soils and Saprolites Involving Formation of Embryonic Halloysite and Gibbsite at Mt Amiata, Central Italy. *Geoderma*, **133**, 173-190. https://doi.org/10.1016/j.geoderma.2005.07.005

[29] Mongelli, G., Buccione, R. and Sinisi, R. (2015) Genesis of Autochthonous and Allochthonous Apulian Karst Bauxites (Southern Italy): Climate Constraints. *Sedimentary Geology*, **325**, 168-176. https://doi.org/10.1016/j.sedgeo.2015.06.005

[30] Boni, M., Rollinson, G., Mondillo, N., Balassone, G. and Santoro, L. (2013) Quantitative Mineralogical Characterization of Karst Bauxite Deposits in the Southern Apennines, Italy. *Economic Geology*, **108**, 813-833. https://doi.org/10.2113/econgeo.108.4.813

[31] Mongelli, G., Boni, M., Buccione, R. and Sinisi, R. (2014) Geochemistry of the Apulian Karst Bauxites (Southern Italy): Chemical Fractionation and Parental Affinities. *Ore Geology Reviews*, **63**, 9-21. https://doi.org/10.1016/j.oregeorev.2014.04.012

[32] Momo, N.M., Tematio, P. and Yemefack, M. (2012) Multi-Scale Organization of the Doumbouo-Fokoué Bauxites Ore Deposits (West Cameroon): Implication to the landscape Lowering. *Open Journal of Geology*, **2**, 14-24. https://doi.org/10.4236/ojg.2012.21002

[33] Mameli, P., Mongelli, G., Oggiano, G. and Dinelli, E. (2007) Geological, Geochemical and Mineralogical Features of Some Bauxite Deposits from Nurra (Western Sardinia, Italy): Insights on Conditions of Formation and Parental Affinity. *International Journal of Earth Sciences*, **96**, 887-902. https://doi.org/10.1007/s00531-006-0142-2

[34] Gamaletsos, P., Godelitsas, A., Mertzimekis, T.J., Göttlicher, J., Steininger, R., Xanthos, S., Berndt, J., Klemme, S., Kuzmin, A. and Bardossy, G. (2011) Thorium Parti-

tioning in Greek Industrial Bauxite Investigated by Synchrotron Radiation and Laser-Ablation Techniques. *Nuclear Instruments and Methods in Physics Research Section B: Beam Interactions with Materials and Atoms*, **269**, 3067-3073. https://doi.org/10.1016/j.nimb.2011.04.061

[35] Putzolu, F., Papa, A.P., Mondillo, N., Boni, M., Balassone, G. and Mormone, A. (2018) Geochemical Characterization of Bauxite Deposits from the Abruzzi Mining District (Italy). *Minerals*, **8**, Article 298. https://doi.org/10.3390/min8070298

[36] Gu, J., Huang, Z., Fan, H., Jin, Z., Yan, Z. and Zhang, J. (2013) Mineralogy, Geochemistry, and Genesis of Lateritic Bauxite Deposits in the Wuchuan-Zheng'an-Daozhen Area, Northern Guizhou Province, China. *Journal of Geochemical Exploration*, **130**, 44-59. https://doi.org/10.1016/j.gexplo.2013.03.003

[37] Zamaniana, H., Ahmadnejad, F. and Zarasvandi, A. (2016) Mineralogical and Geochemical Investigations of the Mombi Bauxite Deposit, Zagros Mountains, Iran. *Geochemistry*, **76**, 13-37. https://doi.org/10.1016/j.chemer.2015.10.001

[38] Aristizabal, E., Roser, B. and Yokota, S. (2005) Tropical Chemical Weathering of Hillslope Deposits and Bedrock Source in the Aburra Valley, Northern Colombian Andes. *Engineering Geology*, **81**, 389-406. https://doi.org/10.1016/j.enggeo.2005.08.001

[39] Hurst, V. and Pickering, S. (1997) Origin and Classification of Coastal Plain Kaolin, Southeastern USA, and the Role of Groundwater and Microbial Action. *Clays and Clay Minerals*, **45**, 274-285. https://doi.org/10.1346/CCMN.1997.0450215

[40] BRGM (2010) Quelles recherches pour l'avenir? symposium franco-allemand sur l'approvisionnement de l'Europe en matières premières non-énergétiques, document de travail.

[41] Liu, X.F., Wang, Q.F., Feng, Y.W., Li, Z. and Cai, S.H. (2013) Genesis of the Guangou Karstic Bauxite Deposit in Western Henan, China. *Ore Geology Reviews*, **55**, 162-175. https://doi.org/10.1016/j.oregeorev.2013.06.002